

# Low-frequency Probes of the Persistent Radio Sources associated with Repeating FRBs

YASH BHUSARE,<sup>1</sup> YOGESH MAAN,<sup>1</sup> AND AJAY KUMAR<sup>1</sup>

<sup>1</sup>*National Centre for Radio Astrophysics, Tata Institute of Fundamental Research, Post Bag 3, Ganeshkhind, Pune - 411007, India*

## ABSTRACT

The discovery of Persistent Radio Sources (PRSs) associated with three repeating fast radio bursts (FRBs) has provided insight into the local environments of these FRBs. Here, we present deep radio observations of the fields surrounding three highly active repeating FRBs namely, FRB 20220912A, FRB 20240114A, and FRB 20240619D using the upgraded Giant Metrewave Radio Telescope (uGMRT) at low radio frequencies. Towards FRB 20240114A, we report the detection of compact source at 650 MHz with a flux density of  $65.6 \pm 8.1 \mu\text{Jy}/\text{beam}$ . Our measurements of the spectral index, star formation rate of the host galaxy and recently reported constraints on the physical size strongly argue for our detected source to be a persistent radio source (PRS) associated with the FRB 20240114A. For FRB 20220912A, we detect radio emission that is most likely due to star formation in the host galaxy. For FRB 20240619D, we provide upper limits on the radio emission from an associated PRS or the host galaxy. The detection of the PRS associated with FRB 20240114A is a useful addition to the PRSs known to be associated with only three other FRBs so far, and further supports the origin of the PRS in the form of magnetoionic medium surrounding the FRB sources.

*Keywords:* Fast Radio Bursts (2008) — FRBs (2008) — Radio Transients (1868)

## 1. INTRODUCTION

Since their discovery, fast radio bursts (FRBs) (Lorimer et al. 2007) have captured significant interest due to their exotic natures. FRBs are typically categorized into two types, repeaters and one-off events. Repeaters offer an excellent opportunity to study FRBs in detail, including the statistics of various burst properties, their temporal and spectral evolution and energetics (e.g., Zhang et al. 2023; Sand et al. 2023; Li et al. 2019; Collaboration et al. 2023; Kirsten et al. 2023; Kumar et al. 2024). Given the millisecond durations of FRBs, their origins are likely to be compact objects. Analyzing the properties of FRBs provides insights into both the radiation mechanisms involved and the environment surrounding the compact engines that produce them. To explore and characterize the radiative environment around FRBs, deep continuum studies are crucial.

Persistent Radio Sources (PRSs) associated with FRBs are compact and characterized by continuous radio emission, unlike the transient nature of FRBs. To date, PRS associated with three FRBs have been

found, FRB 20121102A (Chatterjee et al. 2017), FRB 20190520B (Niu et al. 2022), and FRB 20201124A (Bruni et al. 2024a). The non-thermal radiation from these PRSs is thought to originate from the environment surrounding the compact object driving the FRB emission. The first two detected PRSs exhibit high luminosity, of the order of  $10^{29}$  erg/s/Hz (Chatterjee et al. 2017; Niu et al. 2022). More recently, Bruni et al. (2024a) reported the detection of a faint PRS associated with FRB 20201124A. The luminosities of these PRSs show a correlation with the Rotation Measure (RM) deduced from bursts, suggesting that the persistent emission is tracing a dense magneto-ionic medium. The relatively high RM observed in the corresponding FRB independently supports this scenario.

Detecting and studying more PRSs could significantly advance our understanding of the origins of FRBs, their local environments, and the nature of the compact objects powering them. The faintness of the newly discovered PRS associated with FRB 20201124A raises the possibility that many more such sources exist but have remained undetected due to observational limitations. It is also possible that some FRBs could be linked to compact objects embedded in magnetized plasma, while others might be located in more diffuse media, leading to different observable properties. In this context, the

study of FRB surroundings is crucial for differentiating these potential models. By probing the local environments of FRBs, we can explore the mechanisms responsible for their emission and better understand, whether the associated PRSs are a universal feature of all (repeating) FRBs or specific to certain progenitor systems.

Given the potential diversity of FRB environments, a detailed study of individual sources is essential to understand the physical mechanisms. In this work, we focus on three highly active repeaters, namely, FRB 20220912A, FRB 20240114A, and FRB 20240619D each offering a unique opportunity to investigate their surrounding environments.

FRB 20220912A, discovered in September 2022, became highly active in October 2022. CHIME/FRB detected 9 bursts from this FRB over three days (McKinnven & Chime/Frb Collaboration 2022), indicating it is a highly active repeating source. The FRB has a dispersion measure of  $219.5 \text{ pc cm}^{-3}$  and the RM is  $0.6 \text{ radians m}^{-2}$ . The high level of activity allowed DSA-110 collaboration to quickly localize the source in the host galaxy at a redshift of 0.077 (Ravi et al. 2023). Following its discovery, it was observed by various other telescopes, including our own observations with the Giant Metrewave Radio Telescope (GMRT) resulting in detection of over 100 bursts in November 2022 (Herrmann 2022; Rajwade et al. 2022; Bhusare et al. 2022). Due to its high activity, we have been continuing our monitoring with GMRT, and leveraging GMRTs capability to simultaneously record timeseries and visibility data (detailed analysis on burst rate and properties will be reported elsewhere).

FRB 20240114A was discovered by the CHIME/FRB Collaboration in January 2024 (Shin & CHIME/FRB Collaboration 2024). Based on the observations from MeerKAT (Tian et al. 2024) and the European Very Long Baseline Interferometry Network (EVN) (Snelders et al. 2024), FRB 20240114A is localized (RA =  $21\text{h}27\text{m}39.835\text{s}$ , Dec =  $+04\text{d}19\text{m}45.634\text{s}$ ) in the galaxy J212739.84+041945.8 at a redshift of  $z=0.13$  (Bhardwaj et al. 2024). Bursts from FRB 20240114A are detected in a wide frequency range from 300 MHz to 6 GHz using various telescopes (e.g., (Ould-Boukattine et al. 2024; Joshi et al. 2024; Limaye & Spitler 2024)), with potential hints of even chromaticity (Kumar et al. 2024). The reported RM of FRB 20240114A is  $338 \text{ rad/m}^2$  (Tian et al. 2024) and its DM is  $527 \text{ pc cm}^{-3}$ .

FRB 20240619D is a repeating source discovered by the MeerTRAP team. They detected three bursts from the source within two minutes on 19 June 2024. These bursts triggered the voltage dump from individual antennas, helping in the localization of the source (Tian

et al. 2024). The MeerTRAP team reported an RM of approximately  $177 \text{ rad/m}^2$  and a DM of  $465.48 \text{ pc cm}^{-3}$ . Kumar et al. (2024) followed up with uGMRT and detected 60 bursts, confirming its activity in low frequency as well. There are two optical sources near the FRB location in the images from the DESI Legacy Survey DR10 (Dey et al. 2019). No redshift information is available for these sources. FRB 20240619D could potentially be associated with either of them or an even fainter galaxy, as mentioned by the MeerTRAP team (Tian et al. 2024).

In this paper, we present a study of the fields in the direction of these three highly active repeating FRBs using the upgraded GMRT (uGMRT). Our primary objective is to search for radio emission around these repeating FRBs that could indicate the presence of a PRS or provide clues about their surrounding environments. In the following sections, we provide a detailed description of the observational setup, followed by the data analysis methods, and finally, we discuss our results and their implications.

## 2. OBSERVATIONS

The observations were carried out using the Band-3 (300–500 MHz) and Band-4 (550–850 MHz) of uGMRT, leveraging its capability for simultaneous timeseries and visibility recording. We have observed all the three FRBs at several epochs, and details of the specific observations used in this work are provided below.

For FRB 20220912A, we conducted observations simultaneously in Band-3 and Band-4 by using a dual sub-array mode. Approximately half the antennas were allocated to each of the frequency bands. Data were collected over eight epochs, spanning from May 1 to September 24, 2023 and 3 epochs were imaged. Throughout all epochs, 2355+498 was used as the phase calibrator. Observation was done with 4096 frequency channels and with 5.3 seconds of integration time.

Observations of FRB 20240619D were conducted in Band-3 and Band-4 separately, on 28 August 2024. We dedicated 68 minutes of on-source time in Band-4 and 71 minutes in Band-3. The phase calibration was performed using 1833-210 and 1830-360, while 3C286 was used as the flux calibrator.

For FRB 20240114A, we utilized a total of four Band-4 observations conducted between June 14 to August 22, 2024, with a total of 10 hours on-source time. These observations utilized 2130+050 as the phase calibrator and 3C48 as the flux calibrator. We also observed in Band-3 at 3 epochs, on 5, 8 and 24 March 2024, with the same sets of calibrators.

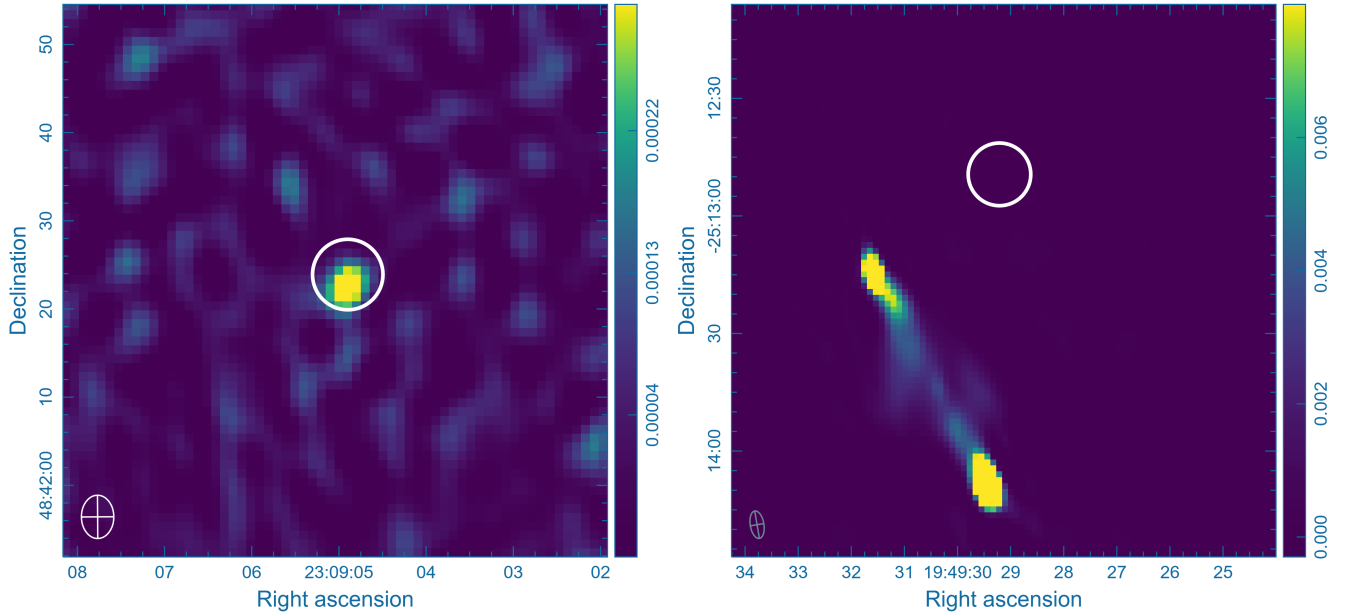


**Figure 1.** The uGMRT Band 4 radio images showing the fields around FRB 20220912A (left) and FRB 20240619D (right). The image of the FRB 20240619D field is limited by dynamic range due to the presence of a nearby bright AGN. Circles indicate the locations of the respective FRBs.

For both FRB 20240114A and FRB 20240619D data was recorded with integration time of 10.7 seconds and 4096 channels in band 4 and 8192 channels in band 3.

### 3. DATA REDUCTION AND ANALYSIS

#### 3.1. Imaging

The uGMRT observations were processed using the CAPTURE pipeline (Kale & Ishwara-Chandra 2020), which uses the Common Astronomy Software Applications (CASA) package. The pipeline begins by initial flagging using CASA tasks like *tfcrop*, aimed at removing radio frequency interference (RFI). It also evaluates the statistics of each antenna, identifying and flagging any bad antennas to ensure good data quality. Following this, primary and secondary calibrations are done using the available calibrator scans. After the first round of calibration, the pipeline conducts another round of flagging, for a better RFI excision. The calibration process is then repeated on the flagged data for further refinement.

Once the calibration is complete, the pipeline processes the target field, applying additional rounds of flagging using CASA tools such as *rflag* and *tfcrop* to clean up the data further. For self-calibration, we utilize an option called *dosubbandselfcal*, which splits the data into different spectral windows, improving the calibration accuracy. We divided the data into 8 to 16 spectral windows during self-calibration. This is followed by multiple rounds of self-calibration, with the dynamic range of the image carefully checked after each round to

ensure progressive improvement. In cases where deconvolution errors appear in the image, manual masking is applied to mitigate these issues and enhance the final image quality.

For FRB 20220912A, our flux calibration scans were not in a usable condition, so we used phase calibrator 2355+498 also as flux calibrator. To model 2355+498 we used measurements given in VLA calibrator list. This approach assumes that flux density is not varying which may not be true. Therefore, we have accounted for an error of up to 30% on flux measurements.

For FRB 20240114A, we conducted a deep search for a radio source by combining four epochs of data, totalling 10 hours of on-source time. After completing all rounds of self-calibration, we merged the datasets to enhance sensitivity. Deconvolution was performed on the combined dataset using both CASA’s *tclean* and WSClean (Offringa et al. 2014) separately, with both algorithms yielding similar results in terms of the residual RMS. Additionally, we imaged two separate parts of Band 4 from the combined data to measure the flux density at two different subbands, each having a bandwidth of 100 MHz.

#### 3.2. Astrometry and Flux density estimation

To ensure accurate astrometry, we cross-matched our dataset with FIRST cutout (Becker 1998) for the field of FRB 20240114A. We used casa task *imfit* to fit and extract the sources from both images. Following this, we conducted a cross-match of the images to identify corresponding sources. Furthermore, we calculated the me-

dian differences separately in right ascension (RA) and declination (DEC) between the reference image and the uGMRT image. These median values were then used to account for any changes in the positions of the sources. For FRB 20240114A, offset was 0.15" in RA and 0.20" in DEC.

We measured the flux density of any particular source using the CASA task *imfit*, specifying the region of the source. This task fits a Gaussian model to the source and the ratio of the peak and integrated flux density estimated from the model also informs about the compactness of the source.

### 3.3. Host galaxy Properties for FRB 20240114A

To derive the host galaxy properties for FRB 20240114A, we utilized public datasets from the Sloan Digital Sky Survey (SDSS; Ahumada et al. 2020) and the Wide-field Infrared Survey Explorer (WISE) (Wright et al. 2010). The host galaxy was detected across all filters of SDSS, and in WISE-filters W1, W3, and W4. We used the "Code Investigating GALaxy Emission" (CIGALE; Boquien et al. 2019) for spectral energy distribution (SED) modeling of the galaxy, enabling us to extract essential parameters such as the star formation rate (SFR) and the mass of the galaxy.

For our analysis, we used the redshift reported by Bhardwaj et al. (2024),  $z = 0.13$ . The star formation history was modeled using a double exponential function, while we utilized the Bruzual & Charlot (2003) stellar population synthesis (SSP) models. Additionally, we included nebular emission and dust attenuation models based on the modified Calzetti et al. (2000) attenuation law, along with the dust emission model by Draine et al. (2014).

## 4. RESULTS

For FRB 20220912A, we imaged data separately for three epochs with on-source times of 49, 77, and 77 minutes observed on May 1, June 2, and July 15, 2023, respectively, at Band 4. The best rms of  $47 \mu\text{Jy}/\text{beam}$  was achieved from the observation on June 2, 2023. In Band 3, we got the best image from the 24<sup>th</sup> march epoch with an rms of  $350 \mu\text{Jy}/\text{beam}$ .

We detected radio emission in the direction of FRB 20220912A at uGMRT Band 4 as shown in Figure 1. The measured flux density is  $435 \pm 53 \mu\text{Jy}/\text{beam}$  (statistical errors only, with systematic errors potentially up to 30%, as we did not have a reliable flux calibrator). No emission was detected at Band 3 of the uGMRT above a  $5\sigma$  level of  $1.750 \text{ mJy}/\text{beam}$ . To estimate the spectral index, we used the publicly available dataset of EVLA from proposal code 22B-307 at C-band. This data was

already pre-processed using the VLA pipeline and we directly used the final image to estimate the flux density at C-band to be  $89 \pm 3.6 \mu\text{Jy}/\text{beam}$ , with an rms of  $3 \mu\text{Jy}/\text{beam}$ . Using this measurement at C-band and our measurement at Band 4 of uGMRT, combined with the uGMRT measurement of  $240 \pm 36 \mu\text{Jy}/\text{beam}$  at 1.26 GHz (Pellicciari et al. 2024) we estimate the spectral index ( $\alpha$ ) to be  $-0.73$ . Previous Very Long Baseline Interferometry (VLBI) observations by Hewitt et al. (2023) did not detect any compact emission from this source above a  $5\sigma$  level of  $80 \mu\text{Jy}$ , leading us to conclude that majority of the radio emission we have detected at Band 4 is likely associated with star formation activity in the host galaxy.

The image towards FRB 20240619D has an rms of  $83.4 \mu\text{Jy}/\text{beam}$ . The FRB position is very close to an Active Galactic Nucleolus (AGN) as shown in figure 1. Due to this nearby bright source, our radio image is limited in dynamic range and we could not probe deep to look for any PRS. Nevertheless, we put a  $5\sigma$  upper limit of  $417 \mu\text{Jy}/\text{beam}$  on a PRS associated with this FRB at 650 MHz. At Band 3, deconvolution errors due to a bright source located between the Full Width at Half Maxima (FWHM) and the first minima of the beam did not allow us to obtain a reasonable quality image.

For FRB 20240114A, our SED modeling of the host galaxy suggests a star formation rate (SFR) of  $0.30 \pm 0.02 \text{ M}_{\odot} \text{ yr}^{-1}$ . Figure 2 shows the best-fit SED of the host galaxy, modeled using CIGALE. The observed photometric data points (purple dots) are fitted with the SED model. The resulting model spectrum is in black. The lower panel shows relative residuals between the observed and modeled fluxes, indicating the goodness of the fit.

Using our radio observations, we report an  $8\sigma$  detection of continuum emission at 650 MHz, potentially from PRS associated with FRB 20240114A. Figure 3 shows the images at band 3 and band 4. We combined observations from 4 epochs between 14 June and 22 August 2024, amounting to a total on-source time of 10 hours. We detected a point source with a peak flux density of  $65.6 \pm 8.1 \mu\text{Jy}/\text{beam}$ . We assume flux density uncertainty of 10% (Chandra & Kanekar 2017) in quadrature with fitting uncertainty for calculating the final error on the flux density. The location of this point source coincides with the location of the FRB. We detected no emission at the FRB position in the Band 3 image. Our best Band 3 image was from the 24 March epoch with an on-source time of 78 minutes, suggests a  $5\sigma$  upper limit of  $600 \mu\text{Jy}/\text{beam}$ . The RMS noise in the Band 3 image is limited by the deconvolution errors caused by

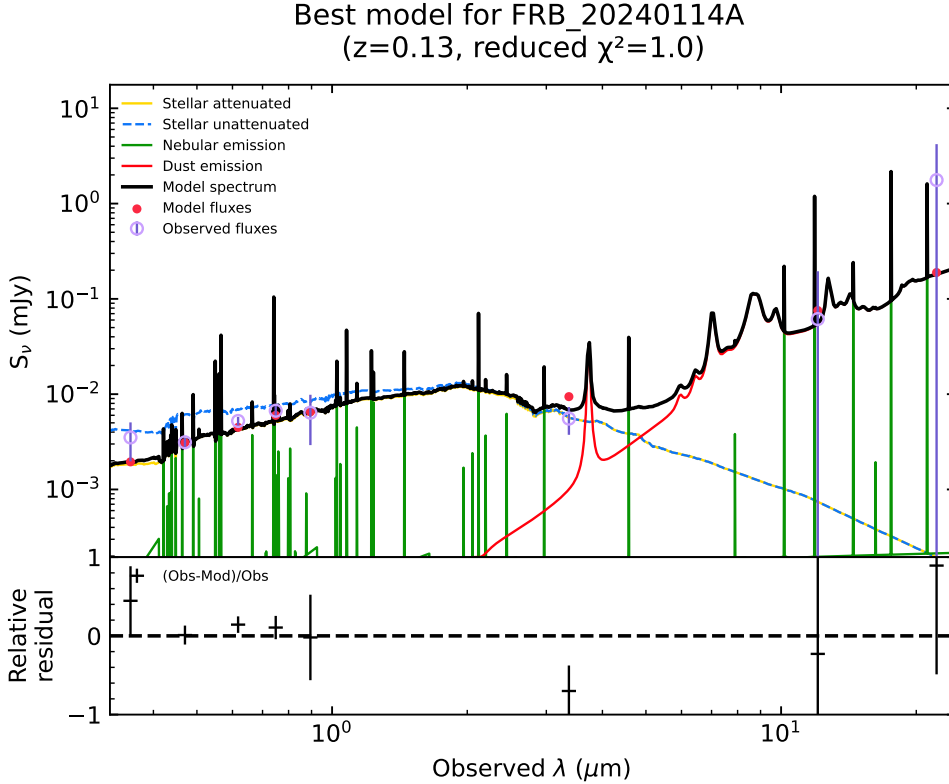


**Figure 2.** SED modeling of the host galaxy of FRB 20240114A using CIGALE. The observed photometric data points (purple dots) from SDSS and WISE are fitted with the model (solid black line) to estimate properties such as the SFR and the stellar mass.

a bright source (325 mJy) located between the FWHM and the first null of the uGMRT primary beam.

## 5. DISCUSSION AND CONCLUSIONS

### 5.1. PRS associated with FRB 20240114A

As a part of our analysis, we estimated the star formation rate (SFR) for the host galaxy of FRB 20240114A using *CIGALE* SED fitting and derived an SFR of  $0.30 \pm 0.02 M_{\odot} \text{yr}^{-1}$ . However, we note that the SFR derived from SPS (Stellar Population Synthesis) using photometric measurements could have limited accuracy due to several factors, e.g., the broadband nature of the filters and dependence on the models used. On the other hand, spectroscopic measurements of the  $H\alpha$  provide a more reliable SFR estimate. Based on spectroscopic data, SFR of the host galaxy is estimated to be  $0.06 \pm 0.01 M_{\odot} \text{yr}^{-1}$  (Xiang-lei Chen, et al.; private communication), indicating that our measurement using the photometric data is an overestimate. Thus, we have used the SFR of  $0.06 M_{\odot} \text{yr}^{-1}$  in any further related discussion or analysis in the rest of this paper.

Using the relation by Garn et al. (2009) with the above SFR estimate and an assumed spectral index of  $-0.8$ , we obtain expected radio luminosity of  $4.3 \mu\text{Jy}$

at 650 MHz and  $2.3 \mu\text{Jy}$  at 1.4 GHz. However, the detected radio emission at 650 MHz is much higher than the above expected from star formation alone — expected star formation emission at 650 MHz is only 6.5% of the observed value. This excess radio flux density suggests the presence of potentially a PRS. We subtract the expected galactic emission due to the star formation ( $4.3 \pm 0.7 \mu\text{Jy}$ ) from the measured flux density ( $65.6 \pm 8.1 \mu\text{Jy}$ ), resulting in the flux density of the potential PRS to be  $61.3 \pm 8.8 \mu\text{Jy}$ .

Some of the earlier searches for any co-located continuum radio emission from FRB 20240114A (e.g., Kumar et al. (2024); Panda et al. (2024) did not reach the required sensitivity to detect the faint emission. However, Zhang & Yu (2024) detected co-located radio continuum at L-band using MeerKAT with flux density of  $72 \pm 14 \mu\text{Jy}$ . Combining our measurement at 650 MHz and the above L-band measurement indicates towards a flat spectrum. Overall, the flat spectrum and the huge excess of radio emission when compared with that expected from the host star formation, makes a strong case for the detected emission to be from a PRS. The more recent detection of a compact source at 5 GHz using VLBA, with a flux density of  $46 \pm 9 \mu\text{Jy}$  and the

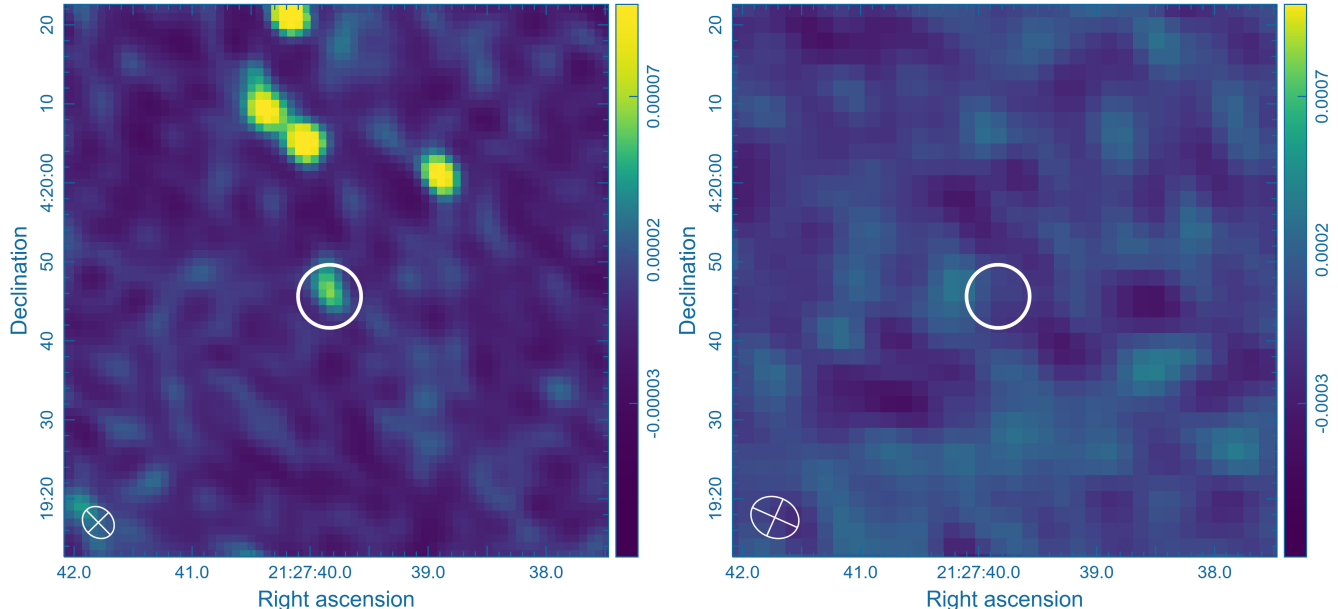


**Figure 3.** Left: A uGMRT Band 4 image of the field around FRB 20240114A, showing a detection of a PRS at the FRB location. Right: Band 3 image of the same field with no detection, limited by relatively large noise. White circles are centered at location of the FRB with a  $4''$  radius.

physical size constrained to  $\lesssim 4$  pc Bruni et al. (2024b), confirms the radio emission to be originated from the PRS associated with FRB 20240114A.

The 5 GHz detection complements our lower-frequency uGMRT observations. Our uGMRT Band 3 image yielded a non-detection with a  $5\sigma$  upper limit of  $600 \mu\text{Jy}$ . In Figure 4, we show all the available flux density measurements, including the measurements and upper limit from this work. Figure 4 also shows the flat spectral nature of the source with a fitted spectral index of  $\alpha = -0.14 \pm 0.12$ , aligning with the characteristics of the other known PRSs. The sub-banded data from uGMRT and MeerKAT might suggest a potential spectral turnover around 1 GHz, however, more precise measurements and ideally at more frequencies would be needed to firmly confirm such a turnover. Nevertheless, if such a turnover is present, it could be due to the synchrotron self-absorption (SSA) or free-free absorption (FFA) from the surrounding environment of FRB. Identifying the cause, SSA or FFA, would help in further determining the characteristics of the FRB environment. SSA would indicate a dense, magnetized region, possibly with a young neutron star or magnetar. FFA, on the other hand, would point towards a dense ionized medium, like a supernova remnant or HII region, which may be between line of sight. In any case, a sensitive and high spatial resolution study of the host galaxy would help in drawing any firm conclusions regarding the spectrum of the candidate PRS.

Using a luminosity distance of 630.72 Mpc (assuming Planck18 cosmology; Astropy Collaboration et al. 2022; Aghanim et al. 2020), we estimate the spectral luminosity of the PRS to be  $2.91 \pm 0.42 \times 10^{28}$  erg/s/Hz. This estimate indicates that the PRS associated with FRB 20240114A is about an order of magnitude fainter compared to those associated with FRB 20121102A and FRB 20190520B. We also analyzed the PRS candidate in the context of the luminosity and rotation measure (RM) relation described by Yang et al. (2022) :

$$L_\nu \propto (\zeta_e \gamma_c^2 R^2) \times |\text{RM}| \quad (1)$$

where,  $\zeta_e$  represents the fraction of electrons emitting synchrotron radiation in the observed frequency band among all electrons,  $\gamma_c$  denotes the Lorentz factor and  $R$  is the radius of the plasma contributing to emission of the PRS as well as the RM.

The other known PRSs are shown to be constrained with  $0.1 < \zeta_e \gamma_c^2 (R/(10^{-2}\text{pc}))^2 < 1.0$  (Bruni et al. 2024a). After subtracting the estimated star formation contribution, the PRS candidate for FRB 20240114A falls just at the upper edge of the above constraints (at an assumed host  $\text{RM}^1$  of  $349 \pm 23 \text{ rad m}^{-2}$ , see Figure 4). Therefore, the PRS associated with FRB 20240114A also follows the constraints followed by the other known PRSs, indicating that the detected emission likely orig-

<sup>1</sup> As estimated by Tian et al. (2024), but we correct for a typo they have in their estimate.

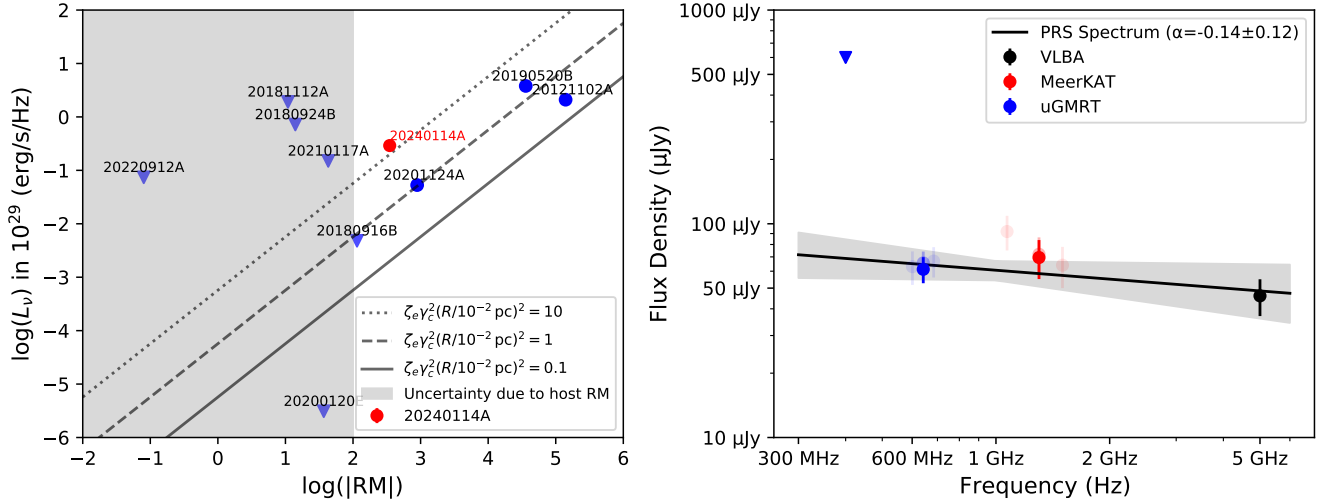


**Figure 4.** Left: A logarithmic plot of the luminosity versus absolute RM adapted from Bruni et al. (2024a), with the addition of FRB 20240114A. The PRS luminosity at 650 MHz is plotted after subtracting the expected contribution from the host galaxy. Right: The radio spectrum of the candidate PRS associated with FRB 20240114A, using measurements from this work at 650 MHz, from Zhang & Yu (2024) at 1.3 GHz and from Bruni et al. (2024b) at 5 GHz. The spectral index is derived from the flux density measurements corrected for the host galaxy emission (dark, filled circles). The fainter points (almost overlapping with the dark points) represent observed values without this correction, while more faded points show the sub-banded measurements, wherever available.

inates from the magneto-ionic region surrounding the FRB, potentially in the form of a magnetar wind nebula.

Although our analysis includes the emission contribution due to the overall SFR of the host galaxy, it would be more useful to measure the SFR specifically at the FRB location to gain a better insight to the environment surrounding the FRB.

### 5.2. FRB 20220912A and FRB 20240619D

We detected radio emission towards FRB 20220912A using uGMRT observations at 650 MHz. As the previous VLBI observations (Hewitt et al. 2023) did not detect any compact radio emission associated with this FRB above a  $5\sigma$  level of  $80 \mu\text{Jy}$ , our uGMRT detection indicates that majority of the detected emission is likely due to star formation within the host galaxy. The SFR for this galaxy, as estimated by Ravi et al. (2023), is greater than  $0.1 M_{\odot} \text{ yr}^{-1}$ . Moreover, the dust-obscured nature of the host galaxy, supported by its position on the WISE color-color plot, also explains the limited optical detections.

The PRS detected by Bruni et al. (2024a) has an inverted spectrum and was found in a star-forming galaxy. Assuming a similar scenario for FRB 20220912A, the star formation emission component could have a steep spectrum, while the PRS contribution might have an inverted or flat spectrum. This would result in the star formation emission dominating at low frequencies, hin-

dering the ability to detect any PRS emission. Our detected radio emission with a spectral index of  $-0.73$  could then indeed correspond to the star formation contribution. Observations at higher frequencies and with higher spatial resolutions would be useful to detect any underlying PRS associated with FRB 20220912A with a flat or inverted spectrum.

For FRB 20240619D, the resulting radio image has an RMS noise level of  $83.4 \mu\text{Jy}/\text{beam}$ . Unfortunately, a nearby active galactic nucleus (AGN), as shown in Figure 1, introduces dynamic range limitations, preventing deeper imaging of the field from searching for any possible PRS. This bright neighbouring source hampers our ability to achieve the desired sensitivity, limiting the detection of any faint PRS. Nevertheless, we put a  $5\sigma$  upper limit of  $417 \mu\text{Jy}/\text{beam}$  on a PRS associated with this FRB at 650 MHz.

Summarizing, we have presented deep low-frequency observations of three highly active repeating FRBs, FRB 20220912A, FRB 20240114A, and FRB 20240619D, using the uGMRT. For FRB 20240114A, we report an  $8\sigma$  detection of a PRS at 650 MHz. The flat radio spectrum, low SFR of the host galaxy and the recently reported physical compactness at 5 GHz corroborate well for the source to be a PRS associated with FRB 20240114A. The measured flux density and a flat spectrum are also consistent with the other known PRSs. The luminosity deduced from our measurements and the RM reported elsewhere, are consistent with

the radio emission to be produced by a magnetoionic medium around the FRB source. For FRB 20220912A, we detected radio emission at 650 MHz, which is consistent with star formation in its host galaxy, as supported by its spectrum as well as the lack of observable compact emission in the previous VLBI studies. In the case of FRB 20240619D, we set upper limit on emission from an associated PRS. Future high-resolution VLBI and multi-frequency observations will be the key to further characterize the properties of the PRS associated with FRB 20240114A and to potentially uncover PRSs associated with the other two FRBs.

## ACKNOWLEDGMENTS

We would like to thank Shriharsh Tendulkar and Visweshwar Ram Marthi for the insightful discussion on FRB 20220912A at the initial stages. YB would like to thank Ramananda Santra and Ruta Kale for valuable discussions on interferometric data analysis, and Pralay Biswas, Rashi Jain and Yogesh Wadadekar for their insights on SED fitting. YM acknowledges support from the Department of Science and Technology via the Science and Engineering Research Board Startup Research Grant (SRG/2023/002657). We would like to thank the Centre Director and the observatory for the prompt time allocation and scheduling of our observations. GMRT is run by the National Centre for Radio Astrophysics of the Tata Institute of Fundamental Research. We acknowledge the Department of Atomic Energy for funding support, under project 12–R&D–TFR–5.02–0700. This publication makes use of data products from the Wide-field Infrared Survey Explorer, which is a joint project of the University of California, Los Angeles, and the Jet Propulsion Laboratory/California Institute of Technology, funded by the National Aeronautics and Space Administration. The National Radio Astronomy Observatory is a facility of the National Science Foundation operated under cooperative agreement by Associated Universities, Inc. Funding for the Sloan Digital Sky Survey V has been provided by the Alfred P. Sloan Foundation, the Heising-Simons Foundation, the National Science Foundation, and the Participating Institutions. SDSS acknowledges support and resources from the Center for High-Performance Computing at the University of Utah. SDSS telescopes are located at Apache Point Observatory, funded by the Astrophysical Research Consortium and operated by New Mexico State University, and at Las Campanas Observatory, operated by the Carnegie Institution for Science. The SDSS web site is [www.sdss.org](http://www.sdss.org). SDSS is managed by the Astrophysical Research Consortium for the Participating Institutions of the SDSS Collaboration, including Caltech, The Carnegie Institution for Science, Chilean National Time Allocation Committee (CNTAC) ratified researchers, The Flatiron Institute, the Gotham Participation Group, Harvard University, Heidelberg University, The Johns Hopkins University, L’Ecole polytechnique fédérale de Lausanne (EPFL), Leibniz-Institut für Astrophysik Potsdam (AIP), Max-Planck-Institut für Astronomie (MPIA Heidelberg), Max-Planck-Institut für Extraterrestrische Physik (MPE), Nanjing University, National Astronomical Observatories of China (NAOC), New Mexico State University, The Ohio State University, Pennsylvania State University, Smithsonian Astrophysical Observatory, Space Telescope Science Institute (STScI), the Stellar Astrophysics Participation Group, Universidad Nacional Autónoma de México, University of Arizona, University of Colorado Boulder, University of Illinois at Urbana-Champaign, University of Toronto, University of Utah, University of Virginia, Yale University, and Yunnan University.



## REFERENCES

- Aghanim, N., Akrami, Y., Ashdown, M., et al. 2020, *Astronomy & Astrophysics*, 641, A6, doi: [10.1051/0004-6361/201833910](https://doi.org/10.1051/0004-6361/201833910)
- Ahumada, R., Prieto, C. A., Almeida, A., et al. 2020, *The Astrophysical Journal Supplement Series*, 249, 3, doi: [10.3847/1538-4365/ab929e](https://doi.org/10.3847/1538-4365/ab929e)
- Astropy Collaboration, Price-Whelan, A. M., Lim, P. L., et al. 2022, *ApJ*, 935, 167, doi: [10.3847/1538-4357/ac7c74](https://doi.org/10.3847/1538-4357/ac7c74)
- Becker, R. 1998, in *The Impact of Near-Infrared Sky Surveys on Galactic and Extragalactic Astronomy*, ed. N. Epchtein (Dordrecht: Springer Netherlands), 257–257
- Bhardwaj, M., Kirichenko, A., & Gil de Paz, A. 2024, *The Astronomer’s Telegram*, 16613, 1
- Bhusare, Y., Kumar, A., Maan, Y., et al. 2022, *The Astronomer’s Telegram*, 15806, 1
- Boquien, M., Burgarella, D., Roehly, Y., et al. 2019, *Astronomy & Astrophysics*, 622, A103, doi: [10.1051/0004-6361/201834156](https://doi.org/10.1051/0004-6361/201834156)
- Bruni, G., Piro, L., Yang, Y.-P., et al. 2024a, A nebular origin for the persistent radio emission of fast radio bursts. <https://arxiv.org/abs/2312.15296>
- Bruni, G., Piro, L., Yang, Y. P., et al. 2024b, Discovery of a PRS associated with FRB 20240114A. <https://arxiv.org/abs/2412.01478>
- Bruzual, G., & Charlot, S. 2003, *Monthly Notices of the Royal Astronomical Society*, 344, 1000, doi: [10.1046/j.1365-8711.2003.06897.x](https://doi.org/10.1046/j.1365-8711.2003.06897.x)
- Calzetti, D., Armus, L., Bohlin, R. C., et al. 2000, *ApJ*, 533, 682, doi: [10.1086/308692](https://doi.org/10.1086/308692)
- Chandra, P., & Kanekar, N. 2017, *ApJ*, 846, 111, doi: [10.3847/1538-4357/aa85a2](https://doi.org/10.3847/1538-4357/aa85a2)
- Chatterjee, S., Law, C. J., Wharton, R. S., et al. 2017, *Nature*, 541, 58–61, doi: [10.1038/nature20797](https://doi.org/10.1038/nature20797)
- Collaboration, T. C., Andersen, B. C., Bandura, K., et al. 2023, *The Astrophysical Journal*, 947, 83, doi: [10.3847/1538-4357/acc6c1](https://doi.org/10.3847/1538-4357/acc6c1)
- Dey, A., Schlegel, D. J., Lang, D., et al. 2019, *AJ*, 157, 168, doi: [10.3847/1538-3881/ab089d](https://doi.org/10.3847/1538-3881/ab089d)
- Draine, B. T., Aniano, G., Krause, O., et al. 2014, *ApJ*, 780, 172, doi: [10.1088/0004-637X/780/2/172](https://doi.org/10.1088/0004-637X/780/2/172)
- Garn, T., Green, D. A., Riley, J. M., & Alexander, P. 2009, *Monthly Notices of the Royal Astronomical Society*, 397, 1101, doi: [10.1111/j.1365-2966.2009.15073.x](https://doi.org/10.1111/j.1365-2966.2009.15073.x)
- Herrmann, W. 2022, *The Astronomer’s Telegram*, 15691, 1
- Hewitt, D. M., Bhandari, S., Marcote, B., et al. 2023, Millisecond Localisation of the Hyperactive Repeating FRB 20220912A. <https://arxiv.org/abs/2312.14490>
- Joshi, P., Medina, A., Earwicker, J. T., et al. 2024, *The Astronomer’s Telegram*, 16599, 1
- Kale, R., & Ishwara-Chandra, C. H. 2020, *Experimental Astronomy*, 51, 95–108, doi: [10.1007/s10686-020-09677-6](https://doi.org/10.1007/s10686-020-09677-6)
- Kirsten, F., Ould-Boukattine, O., Herrmann, W., et al. 2023, Connecting repeating and non-repeating fast radio bursts via their energy distributions. <https://arxiv.org/abs/2306.15505>
- Kumar, A., Maan, Y., & Bhusare, Y. 2024, Varying activity and the burst properties of FRB 20240114A probed with GMRT down to 300 MHz. <https://arxiv.org/abs/2406.12804>
- Kumar, A., Panda, U., Bhusare, Y., et al. 2024, *The Astronomer’s Telegram*, 16745, 1
- Li, B., Li, L.-B., Zhang, Z.-B., et al. 2019, *International Journal of Cosmology, Astronomy and Astrophysics*, 1, 22–32, doi: [10.18689/ijcaa-1000108](https://doi.org/10.18689/ijcaa-1000108)
- Limaye, P., & Spitler, L. 2024, *The Astronomer’s Telegram*, 16620, 1
- Lorimer, D. R., Bailes, M., McLaughlin, M. A., Narkevic, D. J., & Crawford, F. 2007, *Science*, 318, 777, doi: [10.1126/science.1147532](https://doi.org/10.1126/science.1147532)
- McKinven, R., & Chime/Frb Collaboration. 2022, *The Astronomer’s Telegram*, 15679, 1
- Niu, C.-H., Aggarwal, K., Li, D., et al. 2022, *Nature*, 606, 873–877, doi: [10.1038/s41586-022-04755-5](https://doi.org/10.1038/s41586-022-04755-5)
- Offringa, A. R., McKinley, B., Hurley-Walker, N., et al. 2014, *Monthly Notices of the Royal Astronomical Society*, 444, 606–619, doi: [10.1093/mnras/stu1368](https://doi.org/10.1093/mnras/stu1368)
- Ould-Boukattine, O. S., Hessels, J. W. T., Kirsten, F., et al. 2024, *The Astronomer’s Telegram*, 16432, 1
- Panda, U., Roy, J., Bhattacharyya, S., Dudeja, C., & Kudale, S. 2024, Low-frequency, wideband study of an active repeater, FRB 20240114A, with the GMRT. <https://arxiv.org/abs/2405.09749>
- Pellicciari, D., Bernardi, G., Pilia, M., et al. 2024, *A&A*, 690, A219, doi: [10.1051/0004-6361/202450271](https://doi.org/10.1051/0004-6361/202450271)
- Rajwade, K., Wharton, R., Majid, W., et al. 2022, *The Astronomer’s Telegram*, 15791, 1
- Ravi, V., Catha, M., Chen, G., et al. 2023, *The Astrophysical Journal Letters*, 949, L3, doi: [10.3847/2041-8213/acc4b6](https://doi.org/10.3847/2041-8213/acc4b6)
- Sand, K. R., Breitman, D., Michilli, D., et al. 2023, A CHIME/FRB study of burst rate and morphological evolution of the periodically repeating FRB 20180916B. <https://arxiv.org/abs/2307.05839>
- Shin, K., & CHIME/FRB Collaboration. 2024, *The Astronomer’s Telegram*, 16420, 1
- Snelders, M. P., Bhandari, S., Kirsten, F., et al. 2024, *The Astronomer’s Telegram*, 16542, 1

- Tian, J., Rajwade, K. M., Pastor-Marazuela, I., et al. 2024, Monthly Notices of the Royal Astronomical Society, 533, 3174, doi: [10.1093/mnras/stae2013](https://doi.org/10.1093/mnras/stae2013)
- Tian, J., Pastor-Marazuela, I., Stappers, B., et al. 2024, The Astronomer's Telegram, 16690, 1
- Wright, E. L., Eisenhardt, P. R. M., Mainzer, A. K., et al. 2010, AJ, 140, 1868, doi: [10.1088/0004-6256/140/6/1868](https://doi.org/10.1088/0004-6256/140/6/1868)
- Yang, Y.-P., Lu, W., Feng, Y., Zhang, B., & Li, D. 2022, ApJL, 928, L16, doi: [10.3847/2041-8213/ac5f46](https://doi.org/10.3847/2041-8213/ac5f46)
- Zhang, X., & Yu, W. 2024, The Astronomer's Telegram, 16695, 1
- Zhang, Y.-K., Li, D., Zhang, B., et al. 2023, FAST Observations of FRB 20220912A: Burst Properties and Polarization Characteristics. <https://arxiv.org/abs/2304.14665>